Evidence of Rotational Fröhlich Coupling in Polaronic Trions

Maxim Trushin [ORCID],[1] Soumya Sarkar [ORCID],[2] Sinu Mathew [ORCID],[2,*] Sreetosh Goswami,[2] Prasana Sahoo,[3] Yan Wang,[3] Jieun Yang,[3]
Weiwei Li,[3] Judith L. MacManus-Driscoll,[3] Manish Chhowalla,[3] Shaffique Adam,[1,4,5] and T. Venkatesan[2,4,6]

[1]*Centre for Advanced 2D Materials, National University of Singapore, Singapore 117546*
[2]*NUSNNI NanoCore, National University of Singapore, Singapore 117411*
[3]*Department of Materials Science and Metallurgy, University of Cambridge, Cambridge, United Kingdom CB30FS*
[4]*Department of Physics, National University of Singapore, Singapore, 117551*
[5]*Yale-NUS College, Singapore 138527*
[6]*Department of Electrical and Computer Engineering and Materials Science and Engineering,
National University of Singapore, Singapore 117583*

Electrons commonly couple through Fröhlich interactions with longitudinal optical phonons to form polarons. However, trions possess a finite angular momentum and should therefore couple instead to rotational optical phonons. This creates a polaronic trion whose binding energy is determined by the crystallographic orientation of the lattice. Here, we demonstrate theoretically within the Fröhlich approach and experimentally by photoluminescence emission that the bare trion binding energy (20 meV) is significantly enhanced by the phonons at the interface between the two-dimensional semiconductor MoS_2 and the bulk transition metal oxide $SrTiO_3$. The low-temperature binding energy changes from 60 meV in [001]-oriented substrates to 90 meV for [111] orientation, as a result of the counterintuitive interplay between the rotational axis of the MoS_2 trion and that of the $SrTiO_3$ phonon mode.

Introduction.—The quasiparticle concept is a powerful tool for understanding physics of many-body phenomena [1]. The concept was invented a few decades ago to describe a Fermi liquid [2], and later on applied to a broad range of phenomena including superconductivity [3,4], magnetic ordering [5], and the fractional quantum Hall effect [6]. Optically excited two-dimensional (2D) semiconductors contain tightly bound excitons and trions—quasiparticles composed of electrons and holes glued together by Coulomb forces [7]. Recently, yet another exhibit in this quasiparticle zoo—a *polaronic trion* was reported [8]. In this Letter, we demonstrate that a rotational optical (RO) phonon mode is necessary for the trion to engage in polaronic coupling that explains the underlying mechanism leading to formation of polaronic trions and enables significant tunability of trion binding energy (BE), a key to realizing trion based optoelectronics.

In quasiparticle language, the conventional (Fröhlich [9,10]) polaron is an electron dressed with phonons. The energy needed to undress the polaron (i.e., to release the electron) is the polaron BE. Typically, the strongest Fröhlich coupling occurs with longitudinal optical (LO) phonons in polar crystals with a large difference between the static dielectric permittivity and its electronic contribution, such as in $SrTiO_3$ [11,12]. However, the trion-phonon interaction is distinct from coupling of phonons to free electrons. The outer electron in the trion is bound to the excitonic core (see Fig. 1), resulting in a finite angular momentum which enables stronger coupling with RO rather than LO phonon modes. To maximize the effect, the trion's plane of rotation must match the polarization plane created by the RO mode (see Fig. 1). Hence, we can probe polaronic trions by either changing the Fröhlich coupling itself or the angle between rotational planes of the trion and the RO phonon mode. $SrTiO_3$ hosts RO phonons with very low vibration frequency [13] enabling an ideal environment to investigate the rotational Fröhlich coupling with trions. Notably, by changing the $SrTiO_3$ crystal orientation, one can tilt the rotational axis of the RO phonon mode and hence investigate the angular dependence of this coupling.

PL spectroscopy.—Monolayer MoS_2 is grown on single crystal $SrTiO_3$ substrates by chemical vapor deposition [14], and our samples are of comparable quality with those reported previously, see Supplemental Material [15] for sample characterization. We use three different crystallographic orientations of the $SrTiO_3$ substrate to tailor the polaronic effects in 2D MoS_2. Figure 2(a) shows the differential PL emission spectra of the excitonic (right) and trionic (left) peaks in the MoS_2 PL extracted from the Lorentz fitting described in Ref. [15]. We have confirmed that the low energy peak is indeed a trion and does not arise from defect bound excitons through excitation power and electrostatic doping dependent measurements (Figs. S4 and S5 in Ref. [15]). The exciton-trion peak separation is the trion BE we are after. At low temperatures, the trionic peak
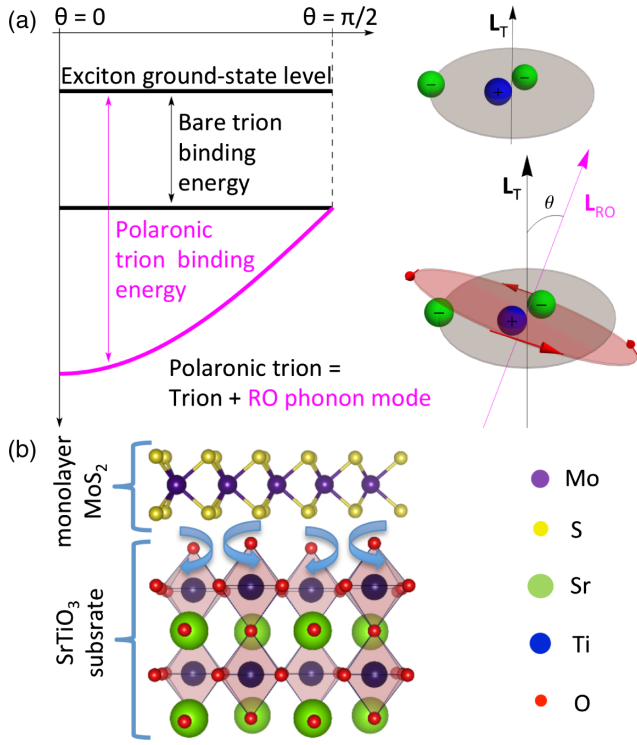
FIG. 1. (a) A trion consists of a tightly bound excitonic core and an electron weakly coupled to the core by the electron-dipole interactions. In a polaronic trion, a RO phonon mode couples with the tangential momentum of the outer electron increasing the resulting quasiparticle BE. The electrons and holes are represented by the green and blue balls, respectively. The tangential polarization generated by the RO phonon mode is shown by the red arrows. The black and magenta arrows show directions of the trion (L_T) and RO phonon (L_{RO}) angular momenta, respectively, and θ is the angle between them. The trion-phonon coupling maximizes at $\theta = 0$ and vanishes at $\theta = \pi/2$, as shown by the polaronic trion BE curve (magenta). The bare trion BE does not depend on θ at all. (b) Schematic of the $MoS_2/SrTiO_3$ heterostructure utilized to create rotational Fröhlich interactions. MoS_2 being an n-type semiconductor exhibits negatively charged trions. At low temperature, $SrTiO_3$ experiences structural cubic-to-tetragonal phase transition that activates the RO phonon mode due to the rotating TiO_6 octahedra (see also Fig. 3).

splits further away from the excitonic peak position, and the splitting turns out to be dependent on the crystallographic orientation of the $SrTiO_3$ substrate. We have achieved BE enhancement of up to 60 meV, that is enormous having in mind that bare trion BE is less than 30 meV. Figure 2(b) shows the full width at half maximum (FWHM) for trionic and excitonic PL peaks. The trion FWHM experiences a significant broadening below the soft phonon activation temperature [13,16] $T_a \sim 132$ K, and the broadening turns out to be strongly dependent on the substrate orientation. In contrast, the exciton FWHM demonstrates much smaller broadening and weaker dependence on the substrate orientation. Finally, the exciton emission energy exhibits the usual monotonic blue shift given by the Varshni relation

[17] whereas the trion emission energy undergoes an unusual red shift below T_a [see Fig. 2(c) and Table S1 in Ref. [15]]. The data presented in Fig. 2 all together indicates that the trion is not a conventional trion anymore but is an entirely new quasiparticle, the polaronic trion [8].

Trion Hamiltonian.—The trion can be seen as an electron weakly interacting with the excitonic core. The unperturbed Hamiltonian describing the relative electron-exciton motion can be written as

$$\hat{H}_0 = -\frac{\hbar^2}{2\mu_T}\left[\frac{1}{r^2}\frac{\partial^2}{\partial\varphi^2} + \frac{1}{r}\frac{\partial}{\partial r}\left(r\frac{\partial}{\partial r}\right)\right]. \quad (1)$$

Here, we use polar coordinates $\{\varphi, r\}$. The trion reduced mass, $\mu_T = m_X m_e/m_T$, is defined in terms of the trion ($m_T = m_X + m_e$), exciton ($m_X = m_e + m_h$), electron (m_e), and hole (m_h) effective masses, respectively. The energy in Eq. (1) is counted from the exciton ground-state level, as shown in Fig. 1(a). The first (second) term in the square brackets is the tangential (radial) momentum operator with the eigenvalues k_φ (k_r) given in units of the Planck constant $\hbar$. The electron-dipole interaction perturbing $\hat{H}_0$ is much weaker than the direct Coulomb potential responsible for the exciton formation and rapidly vanishes at the distances much larger than the exciton size. This results in the trion BE being much lower than that of the exciton.

Rotational Fröhlich coupling.—The 2D Fourier transform of the polaronic interaction can be written as $|V_q|^2 = 8\pi^2 e^2 F^2/q$, where e is the elementary charge, $\mathbf{q}$ is the in-plane wave vector, and F is a proportionality coefficient between the phonon mode amplitude and dielectric polarization created by this mode [18]. To express F in terms of macroscopic quantities we adopt an argument by Kittel [18] where the phonon perturbation producing dielectric polarization is equivalent to the Coulomb potential screened by the phononic part of the dielectric permittivity, i.e.,

$$\frac{2e^2}{\hbar\omega}\sum_{\mathbf{Q}}\frac{(4\pi F)^2}{Q^2}e^{i\mathbf{Q}\cdot\mathbf{r}} = \left(\frac{1}{\epsilon_\infty} - \frac{1}{\epsilon_0}\right)\sum_{\mathbf{q}}\frac{2\pi e^2}{q}e^{i\mathbf{q}\cdot\mathbf{r}}, \quad (2)$$

where ϵ_0 (ϵ_∞) is the static (high-frequency) dielectric permittivity at the $MoS_2/SrTiO_3$ interface, $\hbar\omega$ is the phonon energy quantum, $\mathbf{r}$ is the in-plane coordinate, and $\mathbf{Q}$ is the phonon wave vector whose absolute value can be written in terms of in-plane (q) and axial ($q_\parallel$) components as $Q = \sqrt{q_\parallel^2 + q^2 - 2qq_\parallel\cos(\pi/2 + \theta)}$. The axial component does not contribute to rotational Fröhlich coupling and can be integrated out easily. The resulting polarization turns out to be θ dependent, $F = \sqrt{\hbar\omega\cos\theta(\epsilon_\infty^{-1} - \epsilon_0^{-1})/(8\pi)}$, and the 2D Fourier transform of the polaronic potential reads

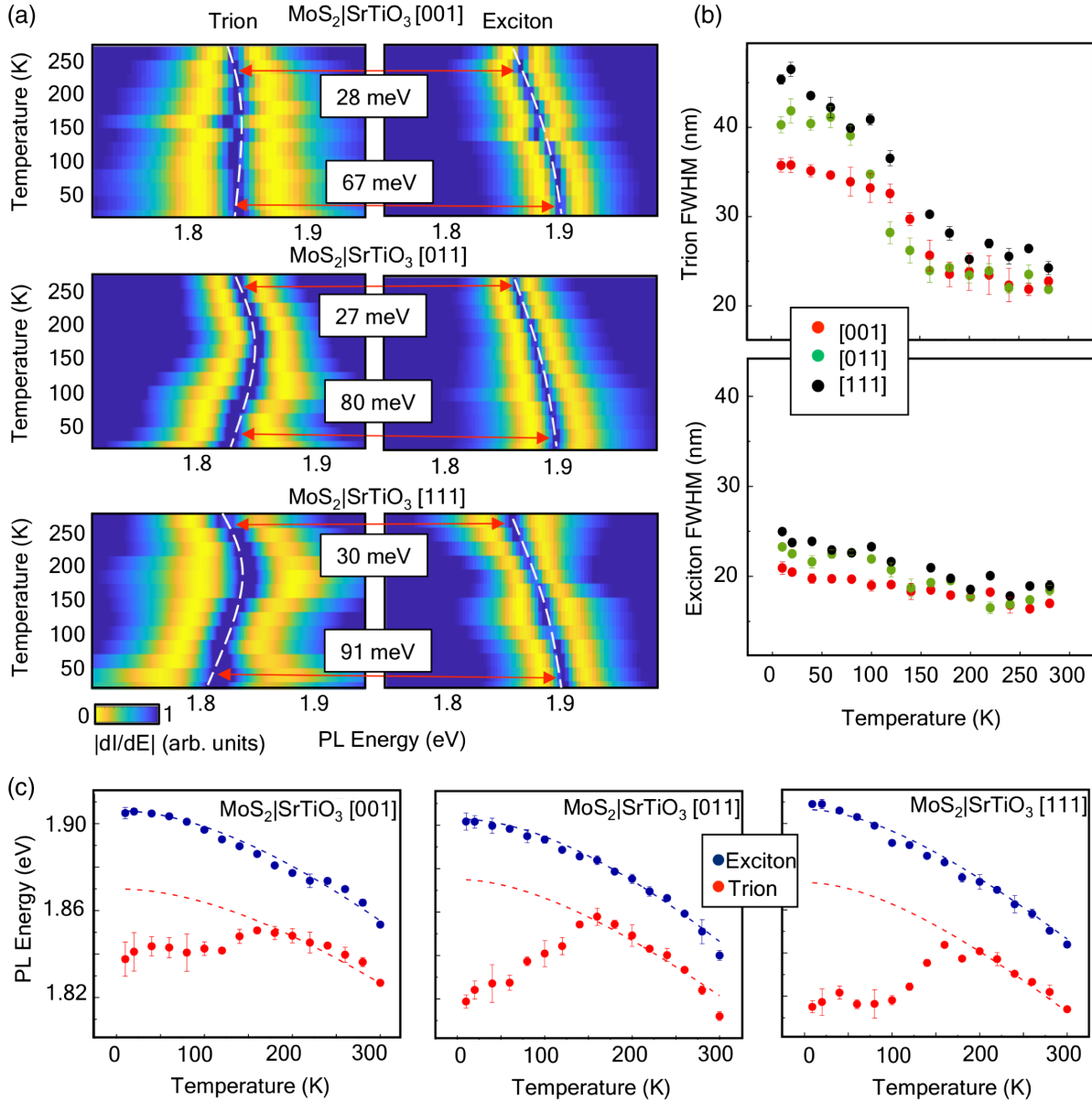FIG. 2. (a) Pseudocolor map of the differential PL emission intensity ($|dI/dE|$) from 2D MoS_2 demonstrates two quasiparticle peaks attributed to excitons and trions. The splitting between them depends on temperature and $SrTiO_3$ substrate orientation with the strongest separation for [111]-oriented $SrTiO_3$ crystals below 50 K. (b) Temperature dependence of FWHM for trionic (upper panel) and excitonic (lower panel) PL quasiparticle peaks for different $SrTiO_3$ substrate orientations indicates much stronger Fröhlich interactions for the former than for the latter. (c) Extracted trionic and excitonic PL energies vs temperature with the corresponding Varshni fits as dashed lines indicate anomalous behavior of the PL trion peak below 132 K. The error bars are the standard error for three samples.

$$V_q = -i\hbar\omega\sqrt{\cos\theta}\sqrt{\frac{2\pi\alpha r_\omega}{q}}, \quad (3)$$

where $r_\omega = \sqrt{\hbar/2\mu_T\omega}$ is the interaction length, and

$$\alpha = \frac{e^2}{2\hbar\omega r_\omega}\left(\frac{1}{\epsilon_\infty} - \frac{1}{\epsilon_0}\right) \quad (4)$$

is the standard Fröhlich coupling constant [9]. The striking difference between the standard 2D polaronic interaction

[11,18] and Eq. (3) is the $\sqrt{\cos\theta}$ prefactor that occurs due to the special direction singled out by the angular momentum of a RO phonon mode. Note that the effective mass in r_ω is given by μ_T instead of m_e as in the conventional case [11].

Polaronic perturbation.—In the nonperturbed limit, when both dipole and polaronic perturbations vanish, the plane-wave solution suggests the kinetic energy $E_{\mathbf{k}}$ of the relative electron-exciton motion be a sum the radial $\hbar^2 k_r^2/2\mu_T$ and tangential $\hbar^2 k_\varphi^2/2\mu_T$ terms. The latter is
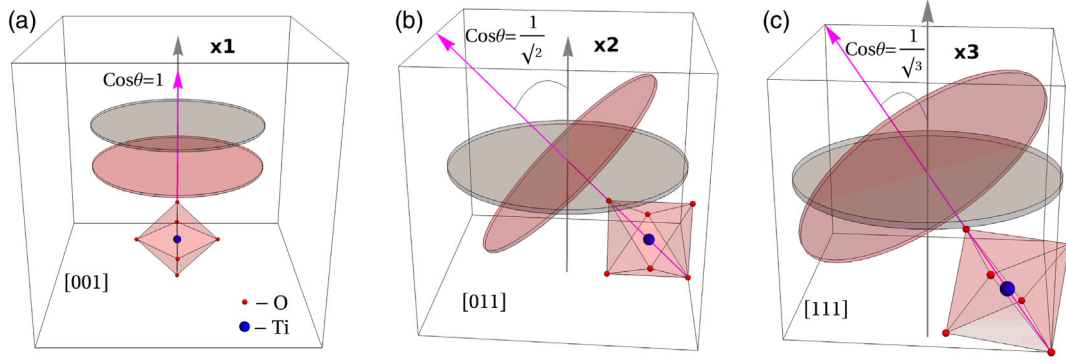
FIG. 3. (a) In a [001]-oriented $SrTiO_3$ domain, the TiO_6 octahedra rotate in the same plane as the trion in 2D MoS_2 placed on top. Here, the trion's and RO phonon planes of rotation are shown by the gray and reddish discs, respectively. (b),(c) Once the $SrTiO_3$ substrate orientation changes, the rotational axes of the trion and RO phonon mode (depicted by black and magenta arrows, respectively) do not align anymore and span the angle θ determined by the domain orientation. The bold numbers indicate the number of mutually perpendicular domain orientations contributing to the polaronic trion BE.

quantized in any circularly symmetric potential, however, we assume that the normalization length is long enough to justify integration instead of summation and map tangential and radial momenta onto the Cartesian coordinates. We note that within the Fröhlich approach, the angular momenta indicated in Fig. 1 are quasiclassical quantities and are not associated with the s and p quantum states. The perturbation theory suggests the following expression for the polaronic energy correction [18]:

$$E_P = -\int \frac{d^2q}{(2\pi)^2} \frac{|V_q|^2}{E_{\mathbf{k}} - E_{\mathbf{k-q}} - \hbar\omega}. \quad (5)$$

We evaluate Eq. (5) for the BE correction ($\mathbf{k} \to 0$). Despite the electron-exciton relative motion being 2D, the rotational polaronic coupling is effectively 1D. This is because RO phonon modes produce no radial polarization [hence, no radial electric field, see Fig. 1(a)], and, therefore, the energy difference $E_{\mathbf{k}} - E_{\mathbf{k-q}}$ does not contain q_r. The BE correction can then be written as

$$E_P = \frac{2}{\pi} \int_0^\infty dq_r \int_0^\infty dq_\varphi \frac{\hbar^2\omega^2 \alpha r_\omega \cos\theta}{\sqrt{q_\varphi^2 + q_r^2}} \frac{2\mu_T/\hbar^2}{q_\varphi^2 + r_\omega^{-2}}$$

$$= \alpha\hbar\omega \cos\theta \ln(2r_\omega/a), \quad (6)$$

where $1/a$ is a momentum cutoff. Similar to the conventional expression for the 2D polaron BE, $E_P = (\pi/2)\alpha\hbar\omega$, our result is linear in α (this also holds beyond perturbation theory, see, e.g., Refs. [11,19,20]) and linear in phonon energy $\hbar\omega$, setting the scale of polaronic interactions. However, Eq. (6) is different in two important ways: since the RO phonon modes are decoupled from both the axial and radial electron motion, this results respectively in the $\cos\theta$ and $\ln(2r_\omega/a)$ prefactors (the latter is a weak function of the order of unity and less important than

the former). The logarithmic divergence is a well-known property of the Fröhlich coupling in a 1D limit [21]. The length a is the lattice constant that determines the first Brillouin zone size in MoS_2. If q_r is retained in the denominator of Eq. (5), and θ is set to zero, we recover the conventional result.

Discussion.—The dressed trion BE is $E_{PT} = E_P + E_T$, where E_T is the bare trion binding energy. To make predictions regarding BE in realistic samples the multi-domain structure of the $SrTiO_3$ substrate must be taken into account. The axis of antiphase rotation of neighboring oxygen TiO_6 octahedra is different in each domain [22]. We assume that the domain orientation is perfectly random, so that any of three mutually perpendicular orientations are weighted equally in the BE calculation. In the simplest case of the [001]-grown substrate, the rotational axis of the RO mode in [001]-oriented domain is normal to the trion plane and the polaronic effect is maximal [see Fig. 3(a)]. The other two [010]- and [100]-oriented domains do not contribute at all because the phonon mode rotation axis is parallel to the trion plane and $\theta = \pi/2$ in Eq. (6). Hence, the total E_{PT} reads

$$E_{PT}[001] = E_T + \alpha\hbar\omega \ln(2r_\omega/a). \quad (7)$$

In the case of either [011] or [101] domain orientation we have $\cos\theta = 1/\sqrt{2}$ [see Fig. 3(b)]. The [110]-oriented domains do not contribute here, and E_{PT} reads

$$E_{PT}[011] = E_T + \sqrt{2}\alpha\hbar\omega \ln(2r_\omega/a). \quad (8)$$

The [111] orientation suggests $\cos\theta = 1/\sqrt{3}$ [see Fig. 3(c)], and all three possible mutually perpendicular domain orientations do contribute equally. Hence, we have
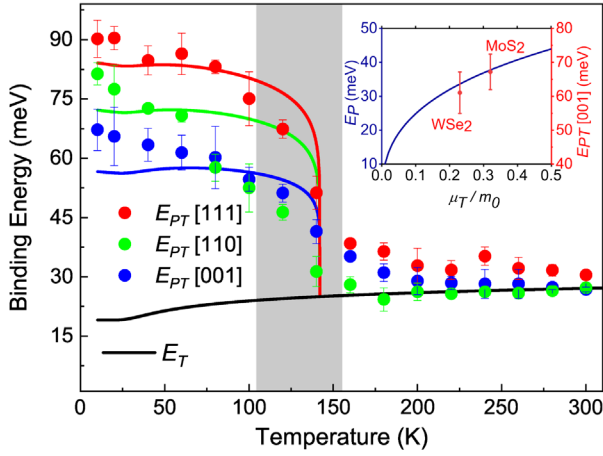
FIG. 4. Temperature dependence of the polaronic trion BE measured for three different substrate orientations along with E_{PT} given by Eqs. (7), (8), and (9), respectively. The shaded transition region corresponds to $T_c^{\text{bulk}} < T < T_c^{\text{surface}}$ with T_c^{bulk} and T_c^{surface} being the bulk and surface structural transition temperatures, respectively [25]. The model is not expected to fit the BE in that region. The bare trion energy [23] (E_T) is shown for comparison. The error bars are the standard error for three samples. Inset: Polaronic trion BE measured at 10 K for MoS_2 and WSe_2 on the same [001]-oriented $SrTiO_3$ substrate (right axis) follows the theoretical trend predicted by Eq. (6) at $T = 0$ (left axis). We avoid plotting theoretical E_{PT}, as we do not know the phenomenological E_T for WSe_2.

$$E_{PT}[111] = E_T + \sqrt{3}\alpha\hbar\omega \ln(2r_\omega/a). \quad (9)$$

The BE is shown in Fig. 4 as a function of temperature for different substrate orientations. The highest BE (~ 90 meV) is achieved for the [111]-grown substrate despite the smallest $\cos\theta = 1/\sqrt{3}$ (hence, the weakest coupling) for [111]-domain orientation. This is almost twice larger than the highest trion BE reported so far in n-doped MoS_2 (~ 40 meV [23], ~ 50 meV [24]). Moreover, the polaronic trion BE allows for 200% tunability (from ~ 30 meV to ~ 90 meV), which far exceeds that possible by conventional electrostatic gating [24]. The bare trion energy E_T (black line) is estimated using the phenomenological approach of Ref. [23]. Equations (7), (8), and (9) combined with the material parameters, $\epsilon_0(T)$, ϵ_∞, and $\omega(T)$, are able to explain the measured polaronic trion BE behavior for all crystallographic orientations of the substrate. We do not adjust the material parameters, see Supplemental Material [15], which also includes Refs. [13,14,16,17,23–40].

The polaronic effect we have discovered is not limited to trions in MoS_2. We have tested a few similar samples where MoS_2 has been substituted by WSe_2 and found the same PL features as shown in Fig. 2. The PL emission from WSe_2 on $SrTiO_3$ at 10 K (see Fig. S7 in Ref. [15]) shows spectral broadening and an anomalous enhancement in the energy separation between the exciton and trion peak (as compared

with the spectra at 300 K), suggesting an increased trion binding energy. The polaronic trion BE in WSe_2 has turned out to be a little lower than in MoS_2, see inset in Fig. 4 for comparison. As the high-frequency dielectric permittivity is the same for both MoS_2 and WSe_2 [29], we attribute this difference to the lower effective mass in WSe_2 [31,33], see Ref. [15] for details.

Outlook.—The polaronic trion discussed here is a complex three-component quasiparticle comprising the exciton core, an electron, and an RO phonon mode coupled together by both Coulomb and Fröhlich interactions, resulting in a large enhancement of the BE. Since the polaronic interaction length r_ω is much larger than the lattice constant, we expect these polaronic trions to only weakly depend on $SrTiO_3$ surface termination [41]. Despite its complexity we have shown that the quasiparticle can live in 2D semiconductors other than MoS_2. We therefore anticipate further discoveries revealing a hierarchy of energy-rich quasiparticles [42] optically excited in 2D semiconductors with unconventional substrates underneath.

*Present address: Department of Physics, S. B. College, Mahatma Gandhi University, Kerala 686101 India.
[1] L. Venema, B. Verberck, I. Georgescu, G. Prando, E. Couderc, S. Milana, M. Maragkou, L. Persechini, G. Pacchioni, and L. Fleet, Nat. Phys. 12, 1085 (2016).
[2] L. D. Landau, Sov. Phys. JETP 3, 920 (1956).
[3] N. N. Bogoljubov, Il Nuovo Cimento (1955–1965) 7, 794 (1958).
[4] J. G. Valatin, Il Nuovo Cimento (1955–1965) 7, 843 (1958).
[5] A. V. Chumak, V. I. Vasyuchka, A. A. Serga, and B. Hillebrands, Nat. Phys. 11, 453 (2015).
[6] R. B. Laughlin, Rev. Mod. Phys. 71, 863 (1999).
[7] K. F. Mak and J. Shan, Nat. Photonics 10, 216 (2016).
[8] S. Sarkar, S. Goswami, M. Trushin, S. Saha, M. Panahandeh-Fard, S. Prakash, S. J. R. Tan, M. Scott, K. P. Loh, S. Adam, S. Mathew, and T. Venkatesan, Adv. Mater. 31, 1903569 (2019).
[9] H. Fröhlich, Adv. Phys. 3, 325 (1954).

[10] R. P. Feynman, Phys. Rev. **97**, 660 (1955).

[11] J. T. Devreese, Encycl. Appl. Phys. **14**, 383 (1996), https://arxiv.org/abs/cond-mat/0004497.

[12] H. Takashima, R. Wang, B. Prijamboedi, A. Shoji, and M. Itoh, Ferroelectrics **335**, 45 (2006).

[13] J. Petzelt, T. Ostapchuk, I. Gregora, I. Rychetský, S. Hoffmann-Eifert, A. V. Pronin, Y. Yuzyuk, B. P. Gorshunov, S. Kamba, V. Bovtun, J. Pokorný, M. Savinov, V. Porokhonskyy, D. Rafaja, P. Vaněk, A. Almeida, M. R. Chaves, A. A. Volkov, M. Dressel, and R. Waser, Phys. Rev. B **64**, 184111 (2001).

[14] A. M. Van Der Zande, P. Y. Huang, D. A. Chenet, T. C. Berkelbach, Y. You, G.-H. Lee, T. F. Heinz, D. R. Reichman, D. A. Muller, and J. C. Hone, Nat. Mater. **12**, 554 (2013).

[15] See Supplemental Material at http://link.aps.org/supplemental/10.1103/PhysRevLett.125.086803 for sample characterization and material parameters employed in the model.

[16] P. A. Fleury, J. F. Scott, and J. M. Worlock, Phys. Rev. Lett. **21**, 16 (1968).

[17] Y. Varshni, Physica **34**, 149 (1967).

[18] C. Kittel, *Quantum Theory of Solids* (Wiley, New York, 1987).

[19] S. Das Sarma and B. A. Mason, Ann. Phys. (N.Y.) **163**, 78 (1985).

[20] W. Xiaoguang, F. M. Peeters, and J. T. Devreese, Phys. Rev. B **31**, 3420 (1985).

[21] F. M. Peeters and M. A. Smondyrev, Phys. Rev. B **43**, 4920 (1991).

[22] Y.-Y. Pai, A. Tylan-Tyler, P. Irvin, and J. Levy, Rep. Prog. Phys. **81**, 036503 (2018).

[23] Y. Lin, X. Ling, L. Yu, S. Huang, A. L. Hsu, Y.-H. Lee, J. Kong, M. S. Dresselhaus, and T. Palacios, Nano Lett. **14**, 5569 (2014).

[24] K. F. Mak, K. He, C. Lee, G. H. Lee, J. Hone, T. F. Heinz, and J. Shan, Nat. Mater. **12**, 207 (2013).

[25] Z. Salman, M. Smadella, W. A. MacFarlane, B. D. Patterson, P. R. Willmott, K. H. Chow, M. D. Hossain, H. Saadaoui, D. Wang, and R. F. Kiefl, Phys. Rev. B **83**, 224112 (2011).

[26] D. K. Efimkin and A. H. MacDonald, Phys. Rev. B **95**, 035417 (2017).

[27] E. Sawaguchi, A. Kikuchi, and Y. Kodera, J. Phys. Soc. Jpn. **17**, 1666 (1962).

[28] J. H. Barrett, Phys. Rev. **86**, 118 (1952).

[29] A. Laturia, M. L. Van de Put, and W. G. Vandenberghe, npj 2D Mater. Appl. **2**, 6 (2018).

[30] C. Lasota, C.-Z. Wang, R. Yu, and H. Krakauer, Ferroelectrics **194**, 109 (1997).

[31] T. C. Berkelbach, M. S. Hybertsen, and D. R. Reichman, Phys. Rev. B **88**, 045318 (2013).

[32] N. Lu, H. Guo, L. Wang, X. Wu, and X. C. Zeng, Nanoscale **6**, 4566 (2014).

[33] M. Luisier, A. Szabo, C. Stieger, C. Klinkert, S. Brück, A. Jain, and L. Novotny, in *Proceedings of the 2016 IEEE International Electron Devices Meeting (IEDM)* (IEEE, 2016), pp. 5.4.1–5.4.4, https://ieeexplore.ieee.org/document/7838353.

[34] N. Wakabayashi, H. G. Smith, and R. M. Nicklow, Phys. Rev. B **12**, 659 (1975).

[35] C. Lee, H. Yan, L. E. Brus, T. F. Heinz, J. Hone, and S. Ryu, ACS Nano **4**, 2695 (2010).

[36] S. Tongay, J. Suh, C. Ataca, W. Fan, A. Luce, J. S. Kang, J. Liu, C. Ko, R. Raghunathanan, J. Zhou et al., Sci. Rep. **3**, 2657 (2013).

[37] W. Zhao, Z. Ghorannevis, K. K. Amara, J. R. Pang, M. Toh, X. Zhang, C. Kloc, P. H. Tan, and G. Eda, Nanoscale **5**, 9677 (2013).

[38] K. He, N. Kumar, L. Zhao, Z. Wang, K. F. Mak, H. Zhao, and J. Shan, Phys. Rev. Lett. **113**, 026803 (2014).

[39] V. Chellappan, A. L. C. Pang, S. Sarkar, Z. E. Ooi, and K. E. J. Goh, Electron. Mater. Lett. **14**, 766 (2018).

[40] A. M. Jones, H. Yu, N. J. Ghimire, S. Wu, G. Aivazian, J. S. Ross, B. Zhao, J. Yan, D. G. Mandrus, D. Xiao et al., Nat. Nanotechnol. **8**, 634 (2013).

[41] A. Schrott, J. Misewich, M. Copel, D. Abraham, and Y. Zhang, Appl. Phys. Lett. **79**, 1786 (2001).

[42] M. Barbone, A. R.-P. Montblanch, D. M. Kara, C. Palacios-Berraquero, A. R. Cadore, D. De Fazio, B. Pingault, E. Mostaani, H. Li, B. Chen et al., Nat. Commun. **9**, 3721 (2018).